

Informative Path Planning with Guaranteed Estimation Uncertainty

Kalvik Jakkala

Saurav Agarwal

Jason O’Kane

Srinivas Akella

Abstract—Environmental monitoring robots often need to reconstruct spatial fields (e.g., salinity, temperature, bathymetry) under tight distance and energy constraints. Classical boustrophedon lawnmower surveys provide geometric coverage guarantees but can waste effort by oversampling predictable regions. In contrast, informative path planning (IPP) methods leverage spatial correlations to reduce oversampling, yet typically offer no guarantees on reconstruction quality. This paper bridges these approaches by addressing *informative path planning with guaranteed estimation uncertainty*: computing the shortest path whose measurements ensure that the Gaussian-process (GP) posterior variance—an intrinsic uncertainty measure that lower-bounds the mean-squared prediction error under the GP model—falls below a user-specified threshold over the monitoring region.

We propose a three-stage approach: (i) learn a GP model from available prior information; (ii) transform the learned GP kernel into binary *coverage maps* for each candidate sensing location, indicating which locations’ uncertainty can be reduced below a specified target; and (iii) plan a near-shortest route whose combined coverage satisfies the global uncertainty constraint. To address heterogeneous phenomena, we incorporate a nonstationary kernel that captures spatially varying correlation structure, and we accommodate non-convex environments with obstacles. Algorithmically, we present methods with provable approximation guarantees for sensing-location selection and for the joint selection-and-routing problem under a travel budget. Experiments on real-world topographic data show that our planners meet the uncertainty target using fewer sensing locations and shorter travel distances than a recent baseline, and field experiments with bathymetry-mapping autonomous surface and underwater vehicles demonstrate real-world feasibility.

I. INTRODUCTION

Monitoring key environmental variables—such as ocean currents, soil moisture, ocean salinity, tree cover, and bathymetry—is a critical task of paramount importance [3]. These quantities are both sensitive indicators and active drivers of coupled Earth-system dynamics that shape climate, hazards, ecosystems, and resource availability. Systematic observations that provide robustness through model-based guarantees, efficiency through resource-aware optimization, and repeatability through automation are therefore essential for effective risk reduction and sustainable management.

Despite its importance, environmental monitoring under finite resources is anything but straightforward. Consider deploying an autonomous surface vehicle (ASV) to measure salinity in a large lake. Salinity is not static: it evolves with rainfall, runoff, wind-driven mixing, and seasonal turnover. A single pass thus offers only a snapshot; meaningful monitoring requires repeated mapping, often on tight timelines. To keep pace, the ASV may need to operate continuously, supported by personnel responsible for mission planning,

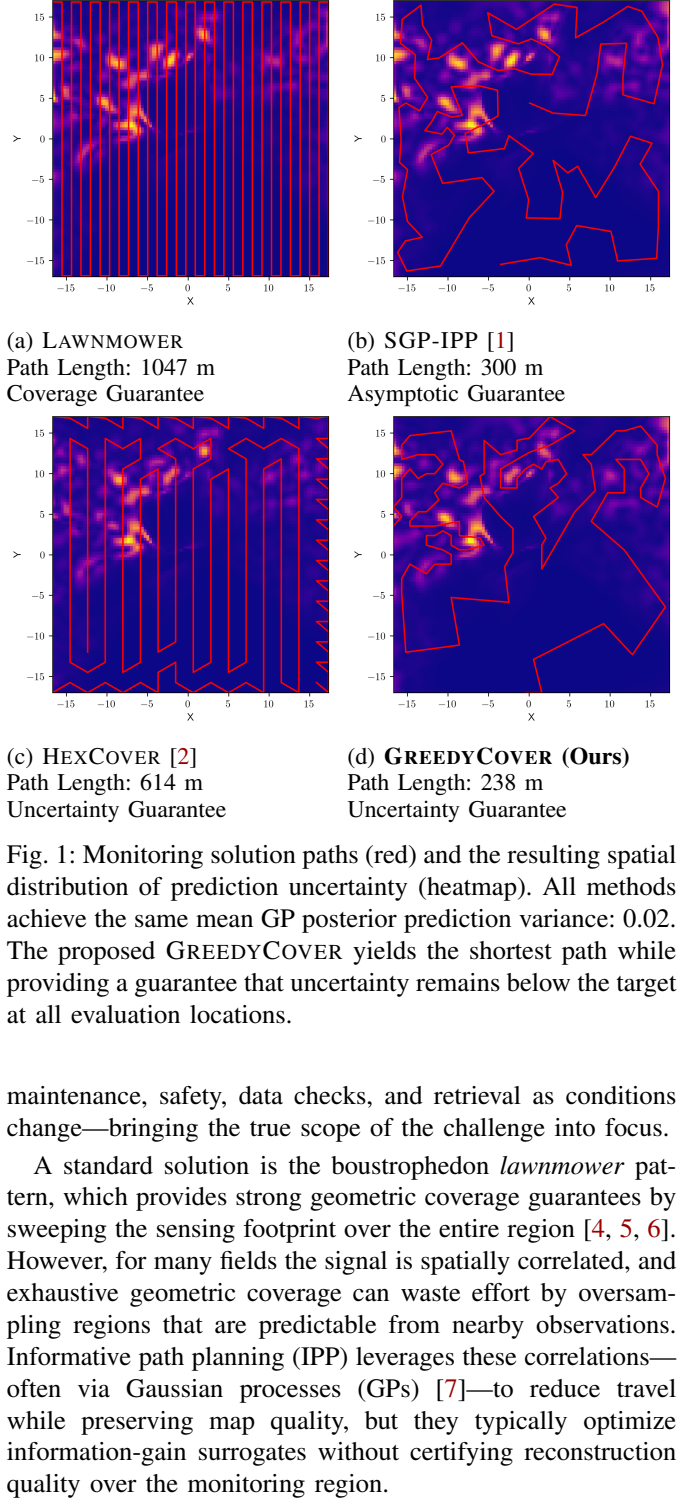


Fig. 1: Monitoring solution paths (red) and the resulting spatial distribution of prediction uncertainty (heatmap). All methods achieve the same mean GP posterior prediction variance: 0.02. The proposed GREEDYCOVER yields the shortest path while providing a guarantee that uncertainty remains below the target at all evaluation locations.

maintenance, safety, data checks, and retrieval as conditions change—bringing the true scope of the challenge into focus.

A standard solution is the boustrophedon *lawnmower* pattern, which provides strong geometric coverage guarantees by sweeping the sensing footprint over the entire region [4, 5, 6]. However, for many fields the signal is spatially correlated, and exhaustive geometric coverage can waste effort by oversampling regions that are predictable from nearby observations. Informative path planning (IPP) leverages these correlations—often via Gaussian processes (GPs) [7]—to reduce travel while preserving map quality, but they typically optimize information-gain surrogates without certifying reconstruction quality over the monitoring region.



Fig. 2: An autonomous surface vehicle (ASV) and an autonomous underwater vehicle (AUV) mapping bathymetry during our field trials.

Recent work has begun to bridge this gap by providing *estimation-uncertainty guarantees*, which bound the mean-squared prediction error by bounding the GP posterior variance [8, 2]. These methods effectively retain coverage-style certification while leveraging GP structure, but they are limited in two key ways: they assume a *stationary* correlation model via a Radial Basis Function (RBF) kernel [7], and existing guarantees are derived for simplified convex environments. Both assumptions are frequently violated in real deployments, where fields can be highly non-stationary and monitoring regions are often non-convex and contain obstacles.

This paper addresses these limitations by developing new methods for IPP with estimation-uncertainty guarantees. Figure 1 highlights the resulting efficiency gains in a non-stationary bathymetry setting relative to representative baselines. Our contributions are as follows:

- We present an informative path planning (IPP) approach that *guarantees the maximum predictive uncertainty* is below a user-specified threshold.
- We introduce an approach that captures and leverages *non-stationary correlations*, while also accommodating *non-convex environments* with known obstacles and complex geometries.
- We provide *near-optimal approximation algorithms* for (i) sensing-location selection and (ii) the joint problem of sensing-location selection and route planning.
- We validate the approach through *field trials* with bathymetry-mapping autonomous surface and underwater vehicles, demonstrating real-world feasibility.

II. RELATED WORK

Lawnmower-style coverage planners: A common approach in environmental monitoring is the boustrophedon *lawnmower* sweep, where a robot follows parallel transects that deterministically cover the environment with the sensing footprint [4]. This paradigm has been studied under realistic vehicle constraints such as Dubins kinematics constraints for surface vehicles [5], and extended to multi-robot settings where practical constraints such as limited onboard capacity must be respected while maintaining area coverage objectives [6].

Contrast to our work: Lawnmower planners guarantee geometric coverage but ignore spatial correlations, often over-sampling predictable regions. We instead plan to satisfy a

worst-case GP posterior-uncertainty threshold, enabling non-sweep paths that reduce redundant sampling while certifying reconstruction quality.

Coverage planners: Our problem is also closely related to viewpoint and sensor placement formulations that provide geometric alternatives to sweeping, such as randomized art-gallery algorithms for selecting sensor locations that collectively *see* an environment [9]. More broadly, coverage planning includes decentralized and adaptive strategies that target geometric visitation or sensing density objectives, particularly in complex environments and multi-robot settings. For example, Voronoi-based approaches provide coverage guarantees in non-convex environments with networked robot teams [10], and robust adaptive coverage control addresses uncertainty in sensor network coverage objectives [11]. In unknown environments, adaptive coverage methods trade off exploration (discovering free space) with coverage progress to improve efficiency [12].

Contrast to our work: These methods primarily enforce geometric visitation/visibility objectives and optimize motion-centric costs, without certifying field reconstruction quality. Our work targets a GP-based *coverage-as-uncertainty* requirement by imposing a global worst-case posterior variance threshold over the region.

Informative path planning methods: Informative Path Planning (IPP) and robotic information gathering (RIG) plan paths to maximize information about an unknown field, commonly using Gaussian processes (GPs) [7] to model spatial structure. Submodular formulations have enabled efficient approximation algorithms for sensor placement and informative sampling, including classical GP-based sensor placement guarantees [13] and robotics formulations with travel/routing constraints [14, 15].

Within robotics, IPP has been studied for waypoint optimization in spatiotemporal monitoring [16], adaptive continuous-space IPP for online environmental monitoring [17], and Bayesian exploration for mapping objectives [18]. More recent optimization-based methods include sequential and approximate approaches to IPP [19], and extensions to heterogeneous robot teams, such as wavelet-based distributed mapping combined with ergodic exploration [20]. Learning-based techniques have also gained traction, including deep RL for adaptive informative planning [21] and learned adaptive navigation for scalar field mapping and feature tracking [22]. Complementary lines of work emphasize selective or structured sampling patterns, for example multi-scale paths for marine vehicles [23]. Meanwhile, improved model expressiveness and scalability have been pursued through kernel learning, including attentive kernels for information gathering [24] and probabilistic online attentive mapping [25]. In parallel, recent work has cast IPP and sensor placement as differentiable optimization problems using sparse Gaussian processes [26, 27, 1], and has applied routing-constrained IPP to domain-specific estimation tasks such as gas leak rate estimation [28].

Contrast to our work: Many IPP approaches optimize information-gain surrogates (e.g., mutual information or entropy reduction) without guarantees on reconstruction quality.

We instead plan around an explicit *global uncertainty constraint* and design algorithms to satisfy it efficiently.

IPP methods with estimation uncertainty guarantees: A key motivation for our work is the comparatively small set of IPP methods that provide *estimation-uncertainty guarantees*—i.e., methods that certify the reconstructed field meets a user-specified uncertainty, rather than merely improving an aggregate information metric. Suryan and Tokekar study learning a spatial field in minimum time with a team of robots, leveraging GP structure and deriving performance guarantees for multi-robot sampling under time constraints [8]. Building on this foundation, Dutta *et al.* present approximation algorithms for the associated sample-placement and shortest-path problems in convex environments, strengthening prior theoretical guarantees [2]. Together, these works demonstrate that coverage-style certification can be integrated with informative sampling.

Contrast to our work: Prior guarantee-bearing methods typically assume a *single stationary* correlation structure and derive guarantees for simplified convex geometries, which can be mismatched to spatially varying fields and obstacle-rich domains. We support expressive (including non-stationary) correlation models and enforce the same worst-case uncertainty requirement in *non-convex environments with known obstacles*, while also providing near-optimal approximation guarantees.

III. PRELIMINARIES: GAUSSIAN PROCESSES

We model the monitored quantity as an unknown function over a domain and use Gaussian processes (GPs) [7] to represent both spatial structure and predictive uncertainty.

GP prior: A Gaussian process is a stochastic process such that any finite collection of function values is jointly Gaussian. Equivalently, a GP induces a distribution over functions, making it a flexible Bayesian prior for regression. We place a GP prior on the latent field $f(\cdot)$:

$$f(x) \sim \mathcal{GP}(m(x), k(x, x')), \quad (1)$$

where $m(x)$ is the mean function (often taken to be 0 after normalization) and kernel $k(x, x')$ is a positive semi-definite covariance function. The kernel specifies prior correlations:

$$k(x, x') = \text{cov}(f(x), f(x')). \quad (2)$$

Noisy observations and posterior prediction: Given n noisy samples $\mathcal{D} = \{(x_i, y_i)\}_{i=1}^n$ with $y_i = f(x_i) + \varepsilon_i$ and i.i.d. Gaussian noise $\varepsilon_i \sim \mathcal{N}(0, \sigma_n^2)$, define the stacked training inputs $X = [x_1, \dots, x_n]$ and outputs $y = [y_1, \dots, y_n]^\top$. For a query location x_* , GP regression yields a Gaussian predictive distribution $p(f_* | X, y, x_*) = \mathcal{N}(\mu_*, \sigma_*^2)$, with

$$\mu_* = K_{*n} (K_{nn} + \sigma_n^2 I)^{-1} y, \quad (3)$$

$$\sigma_*^2 = K_{**} - K_{*n} (K_{nn} + \sigma_n^2 I)^{-1} K_{n*}. \quad (4)$$

Here, K_{nn} is the $n \times n$ covariance matrix with $(K_{nn})_{ij} = k(x_i, x_j)$, K_{*n} is the $1 \times n$ vector with $(K_{*n})_i = k(x_*, x_i)$, $K_{n*} = K_{*n}^\top$, and $K_{**} = k(x_*, x_*)$. The posterior variance σ_*^2 provides an intrinsic uncertainty measure that depends only

on the input locations (and the GP hyperparameters), which makes it especially useful for planning.

IV. PROBLEM: INFORMATIVE PATH PLANNING WITH GUARANTEED ESTIMATION UNCERTAINTY

A robot is tasked with monitoring an environmental field (e.g., temperature, radiation, or chemical concentration) over a domain $\mathcal{X} \subset \mathbb{R}^d$, which may be purely spatial or spatio-temporal. For planning and evaluation, we discretize \mathcal{X} into a finite set of *evaluation points* $\mathcal{V} = \{x_1, \dots, x_N\} \subset \mathcal{X}$, at which accurate estimates are required.

Due to accessibility, safety, or operational constraints, the robot can take measurements only at a restricted set of *candidate sensing locations* $\mathcal{C} = \{c_1, \dots, c_M\} \subseteq \mathcal{X}$. A feasible robot path is represented by an *ordered* sequence of waypoints $\mathcal{P} = (p_1, \dots, p_T)$, $p_t \in \mathcal{C}$, and we denote its travel cost by $\text{length}(\mathcal{P})$ (e.g., Euclidean TSP length or boundary-constrained length from sampling-based planners).

Risk criterion: Let $\text{MSE}(x_i | \mathcal{P})$ denote the pointwise mean squared estimation error at $x_i \in \mathcal{V}$ after executing \mathcal{P} and incorporating the measurements obtained from the path. We measure worst-case estimation performance by

$$\text{MSE}_{\max}(\mathcal{P}) := \max_{x_i \in \mathcal{V}} \text{MSE}(x_i | \mathcal{P}). \quad (5)$$

Our objective is to minimize travel cost while guaranteeing that the worst-case error does not exceed a prescribed threshold σ_{tar}^2 —the user-specified target upper bound on the allowable worst-case error, i.e., $\text{MSE}_{\max}(\mathcal{P}) \leq \sigma_{\text{tar}}^2$. Optionally, the robot may also be subject to a travel budget D .

Starting Condition: We are given a sparse, representative set of labeled points in the domain \mathcal{X} , obtained from a pilot mission, historical data, coarse satellite observations, or expert knowledge (e.g., physics-based models).

GP-based surrogate: Directly optimizing $\text{MSE}_{\max}(\mathcal{P})$ is challenging because $\text{MSE}(x_i | \mathcal{P})$ depends on the (unknown) measurements that will be realized along \mathcal{P} . To obtain a tractable planning objective computable from available prior information, we model the unknown field $f : \mathcal{X} \rightarrow \mathbb{R}$ as a Gaussian process (GP). Noisy measurements taken along \mathcal{P} induce a GP posterior with variance $\sigma_{\text{post}}^2(\cdot | \mathcal{P})$. The GP posterior variance lower-bounds the pointwise MSE [29]. We therefore use the conservative surrogate

$$J_{\max}(\mathcal{P}) := \max_{x_i \in \mathcal{V}} \sigma_{\text{post}}^2(x_i | \mathcal{P}) \quad (6)$$

for worst-case estimation error.

Problem: The informative path planning problem with guaranteed estimation uncertainty is:

$$\begin{aligned} \mathcal{P}^* \in \arg \min_{\mathcal{P} \in \mathcal{C}^*} & \text{length}(\mathcal{P}) \\ \text{s.t. } & J_{\max}(\mathcal{P}) \leq \sigma_{\text{tar}}^2, \\ & \text{length}(\mathcal{P}) \leq D \quad (\text{optional}), \end{aligned} \quad (7)$$

where $\mathcal{C}^* := \bigcup_{T \geq 1} \mathcal{C}^T$ denotes the set of all finite waypoint sequences over \mathcal{C} . That is, we seek a minimum-cost sensing path whose measurements guarantee that the posterior uncertainty at every evaluation point is at most σ_{tar}^2 .

V. NEAR-OPTIMAL INFORMATIVE PATH PLANNING

This section presents our approach to solving the informative path planning problem with guaranteed estimation uncertainty. We first describe how we leverage available prior information to compute coverage maps. We then use these maps in two algorithms—GREEDYCOVER and GCBCOVER—which address sensing-location selection and the joint problem of sensing-location selection and route planning, respectively.

A. Coverage Map Construction Theory

We begin by fitting a Gaussian process (GP) to the available prior information. Depending on the data source, we use either a non-stationary kernel [24] or a physics-informed kernel [30]. Using the learned GP, we construct *coverage maps* that specify which evaluation points $v \in \mathcal{V}$ can be driven below the user-specified target posterior variance σ_{tar}^2 by taking a measurement at a candidate sensing location $c \in \mathcal{C}$.

Ideally, coverage would be evaluated jointly over *sets* of sensing locations, since the posterior variance at an evaluation point depends on all measurements collected from a path. However, informative path planning is NP-hard [16]; exact evaluation would require computing posterior variances for many subsets of the power set of \mathcal{C} , which is computationally infeasible. We therefore adopt a scalable alternative: for each candidate location $c \in \mathcal{C}$, we compute the set of evaluation points that would satisfy the variance threshold if we were to observe *only* at c . These per-location coverage maps can then be combined efficiently during planning.

We justify this construction with the following results. The first provides an explicit prior covariance threshold under which a single measurement at a sensing location can reduce the posterior variance at a given evaluation point below σ_{tar}^2 . The second formalizes the monotonicity property that conditioning on additional measurements can only further reduce posterior variance; hence, the single-location condition yields a conservative coverage region for multi-measurement paths.

Theorem 1 (Minimum Required Prior Covariance).

Let $f \sim \mathcal{GP}(0, k)$ with independent Gaussian observation noise variance σ_n^2 , and consider a single noisy observation at candidate location $c \in \mathcal{C}$. Fix an evaluation location $v \in \mathcal{V}$. For any target posterior variance $\sigma_{\text{tar}}^2 \in (0, k(v, v))$, the condition

$$\sigma_{\text{post}}^2(v | c) \leq \sigma_{\text{tar}}^2$$

holds if and only if

$$|k(c, v)| \geq \sqrt{(k(v, v) - \sigma_{\text{tar}}^2)(k(c, c) + \sigma_n^2)}. \quad (8)$$

Thus, achieving a posterior variance of at most σ_{tar}^2 at v requires that the prior covariance between c and v exceed the threshold in Equation 8.

Please refer to the Appendix for the proof.

Theorem 2 (Variance Reduction with Multiple Locations).

Under the setup of Theorem 1, consider n sensing locations $c_1, \dots, c_n \in \mathcal{C}$. Fix an evaluation location $v \in \mathcal{V}$ and

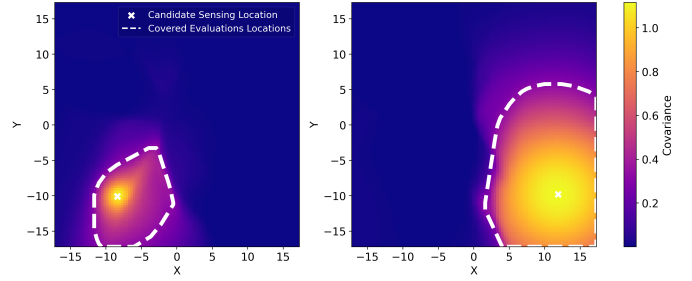


Fig. 3: Coverage maps for two candidate sensing locations under a non-stationary kernel. Each dotted white blob indicates the set of evaluation locations for which that candidate location can guarantee the target posterior-variance threshold.

a target variance $\sigma_{\text{tar}}^2 \in (0, k(v, v))$. Suppose there exists $j \in \{1, \dots, n\}$ such that

$$|k(c_j, v)| \geq \sqrt{(k(v, v) - \sigma_{\text{tar}}^2)(k(c_j, c_j) + \sigma_n^2)}.$$

Then the posterior variance at v conditioned on all observations satisfies

$$\sigma_{\text{post}}^2(v | c_{1:n}) \leq \sigma_{\text{tar}}^2.$$

Please refer to the Appendix for the proof.

B. Binary Coverage Map Construction

Together, Theorems 1 and 2 motivate a per-location notion of coverage: a sensing location c_j covers an evaluation point v_i if the prior covariance $k(c_j, v_i)$ exceeds the threshold in Equation 8. We encode this relationship in a binary matrix $B \in \{0, 1\}^{M \times N}$. For each candidate sensing location $c_j \in \mathcal{C}$ and evaluation point $v_i \in \mathcal{V}$, we set $B_{ji} = 1$ (i.e., sensing at c_j covers v_i) if

$$\mathbb{I}\left\{ |k(c_j, v_i)| \geq \sqrt{(k(v_i, v_i) - \sigma_{\text{tar}}^2)(k(c_j, c_j) + \sigma_n^2)} \right\},$$

and $B_{ji} = 0$ otherwise. Figure 3 shows example coverages.

This binary representation provides two practical benefits. First, it reduces memory compared to storing real-valued covariances for all pairs in $\mathcal{C} \times \mathcal{V}$. Second, it enables fast planning-time updates via set operations: the evaluation points covered by a path can be computed by unions over the rows of B corresponding to the visited candidate locations, without repeatedly evaluating GP posterior variances for different candidate subsets.

C. GREEDYCOVER: IPP via Greedy Selection and TSP

Given the binary coverage matrix B from Section V-B, our first planning approach proceeds in two stages: (i) greedily select a subset of candidate sensing locations that maximizes the number of covered evaluation points, and (ii) construct a path that visits all selected locations using a TSP solver [31].

1) *Greedy Sensor Selection*: Starting from an empty selected set $S_0 = \emptyset$ and an empty covered set $U_0 = \emptyset$, the greedy procedure iteratively adds the candidate location that covers the largest number of *new* (previously uncovered) evaluation points. Let $S_t \subseteq \{1, \dots, M\}$ denote the indices of selected candidates after iteration t , and let $U_t \subseteq \mathcal{V}$ denote the set of evaluation points covered by S_t . The marginal gain of adding candidate index $j \notin S_t$ is

$$\Delta(j \mid S_t) := |\{v_i \in \mathcal{V} : B_{ji} = 1, v_i \notin U_t\}|.$$

At each iteration, we select

$$j^* \in \arg \max_{j \notin S_t} \Delta(j \mid S_t),$$

update $S_{t+1} = S_t \cup \{j^*\}$, and expand the covered set

$$U_{t+1} = U_t \cup \{v_i \in \mathcal{V} : B_{j^*i} = 1\}.$$

The loop terminates once all evaluation points are covered (i.e., $|U_t| = N$) or once no remaining candidate yields additional coverage (i.e., $\max_{j \notin S_t} \Delta(j \mid S_t) = 0$). Algorithm 1 in the Appendix summarizes this procedure. The worst-case running time of the algorithm is $\mathcal{O}(M^2N)$, when $M \leq N$.

2) *Submodularity and Approximation Guarantees*: The objective implicitly optimized by the above greedy method is a classic monotone submodular set function [32, 13]. Define the *coverage function* with $S \subseteq \{1, \dots, M\}$:

$$F(S) := \left| \bigcup_{j \in S} \{v_i \in \mathcal{V} : B_{ji} = 1\} \right|, \quad (9)$$

which counts how many evaluation points are covered by at least one selected candidate. This function is:

- *Monotonically Increasing*: If $Y \subseteq Z$, then $F(Y) \leq F(Z)$, since adding sensing locations can only enlarge the union of covered points.
- *Submodular*: It satisfies diminishing returns. For all $Y \subseteq Z$ and any location $l \notin Z$,

$$F(Y \cup \{l\}) - F(Y) \geq F(Z \cup \{l\}) - F(Z),$$

since the set of newly covered points contributed by l can only shrink as the baseline set grows.

Monotone submodular maximization under a cardinality constraint admits strong approximation guarantees. Given a budget of K sensing locations, the result of Nemhauser *et al.* [32] (Theorem 3 in the Appendix) guarantees that the greedy solution S satisfies

$$F(S) \geq (1 - 1/e) \text{OPT},$$

i.e., it attains at least a $(1 - 1/e) \approx 63\%$ fraction of the optimal coverage OPT achievable with K sensing locations. Thus, the above greedy method provides a provably near-optimal selection with respect to the coverage objective.

3) *Path Construction via TSP*: Given the selected index set S , we construct a low-cost route that visits all sensing locations $\{c_j : j \in S\}$. We treat these locations as nodes in a complete Euclidean graph, with edge weights given by pairwise distances between locations. We then invoke a TSP solver (e.g., the Christofides algorithm [31]) to compute a path through the nodes, which we use as the execution path.

Although our formulation constrains the selected sensing locations to lie within the sensing environment (including non-convex domains), the straight-line edges implied by a Euclidean TSP path may still pass through infeasible space (e.g., outside the boundary or through obstacles). To ensure feasibility, the path can be post-processed using standard motion-planning techniques that replace each straight-line segment with a collision-free, within-bounds path (e.g., via grid-based planning or sampling-based planners) [33].

4) *Limitations of the Decoupled Approach*: This two-stage pipeline—first selecting sensing locations to maximize coverage, then routing them with a TSP solver—has an important limitation: it provides *no joint approximation guarantee* for the combined information–travel objective in Equation 7. The submodular approximation guarantee applies only to maximizing $F(S)$ under a cardinality constraint, and does not account for path length. In practice, greedy selection may choose sensing locations that are geographically dispersed, leading to unnecessarily long routes even though other, slightly different selections could satisfy the estimation uncertainty requirement with a lower travel cost. This limitation motivates our next method, which more tightly couples sensing-location selection and routing.

D. GCBCOVER: IPP via Generalized Cost–Benefit Algorithm

Our second planning method couples sensing-location selection and routing via the generalized cost–benefit (GCB) algorithm [34, 35]. Unlike the decoupled approach, which first maximizes coverage and then computes a path, GCB explicitly trades off *marginal coverage gain* against the *marginal increase in path length* at each iteration.

1) *Generalized Cost–Benefit Selection with Coverage Maps*: We reuse the binary coverage matrix $B \in \{0, 1\}^{M \times N}$ from Section V-B and the coverage function in Equation 9. Let $\text{length}(S)$ denote the routing cost of a selected index set $S \subseteq \{1, \dots, M\}$, defined as the length of a (near-)shortest route that visits the sensing locations $\{c_j : j \in S\}$.

At iteration t , given the current sensing set S_t with coverage $F(S_t)$ and routing cost $\text{length}(S_t)$, each remaining candidate $j \notin S_t$ is scored by a cost–benefit ratio constructed from: (i) the *marginal coverage gain*:

$$\Delta F(j \mid S_t) := F(S_t \cup \{j\}) - F(S_t),$$

and (ii) the *marginal routing-cost increment*:

$$\Delta \text{length}(j \mid S_t) := \text{length}(S_t \cup \{j\}) - \text{length}(S_t).$$

The candidate with the largest ratio:

$$\Delta F(j \mid S_t) / \Delta \text{length}(j \mid S_t)$$

is preferred, subject to feasibility under the distance budget D : candidates that add many newly covered points for a small increase in path length are prioritized.

Because a purely ratio-greedy strategy can be suboptimal under a strict budget, GCB also computes a standard greedy coverage solution and truncates it to satisfy the budget. The algorithm then returns whichever of the budget-feasible solutions attains higher coverage. This comparison step is also necessary for the approximation guarantee stated below. Algorithm 2 in the Appendix summarizes the GCB algorithm.

The worst-case running time is dominated by repeated path length evaluations. Let $T(n)$ denote the time required to compute $\text{length}(\cdot)$ for n sensing locations (e.g., using a TSP algorithm). Using the Christofides algorithm [31], which runs in $T(n) = \mathcal{O}(n^3)$, the resulting worst-case complexity of GCB is $\mathcal{O}(M^2(N + M^3))$, when $M \leq N$.

In our experiments, we use a faster heuristic TSP routine. Starting from an empty path, we estimate path-length increases using a fast incremental heuristic (Algorithm 3 in the Appendix). After selecting each solution sensing location via the GCB ratio, we invoke a full TSP solver to update the path. This strategy improves runtime while retaining solution quality.

2) *Approximation Guarantees Under Routing Constraints*: As discussed in Section V-C, the coverage objective F is monotone submodular. The routing cost $\text{length}(\cdot)$ is a monotone set function defined as the length of a TSP path through the selected sensing locations [34]. The resulting problem fits the standard template of submodular maximization subject to a routing (path-length) constraint:

$$\max_{S \subseteq \{1, \dots, M\}} F(S) \quad \text{s.t.} \quad \text{length}(S) \leq D.$$

The generalized cost-benefit (GCB) algorithm provides a constant-factor guarantee for this class of problems. In particular, under mild conditions on the routing cost function—namely, approximate submodularity with submodularity ratio α_c , bounded curvature κ_c , and a $\psi(n)$ -approximation factor for the TSP solver—the GCB solution satisfies the following bi-criterion guarantee [34] (Theorem 4 in the Appendix):

$$F(S) \geq \frac{1}{2} \left(1 - \frac{1}{e}\right) \text{OPT},$$

where OPT denotes the optimal coverage achievable under a slightly tighter effective budget (with the tightening depending on α_c , κ_c , $\psi(n)$, and the largest feasible solution size). Equivalently, GCB achieves at least a $\frac{1}{2}(1 - 1/e) \approx 31.6\%$ fraction of an *approximate* optimum, where the approximation reflects the quality of the TSP solver. We refer to Zhang and Vorobeychik [34] for a more detailed explanation of the approximation guarantee.

In our setting, F is exactly monotone submodular; thus, all approximation effects arise from the routing component (i.e., the submodularity ratio/curvature of $\text{length}(\cdot)$ and the approximation quality of the TSP solver). Consequently, our method inherits the same worst-case approximation factor as the underlying GCB framework while directly optimizing a coverage objective tailored to informative sensing.

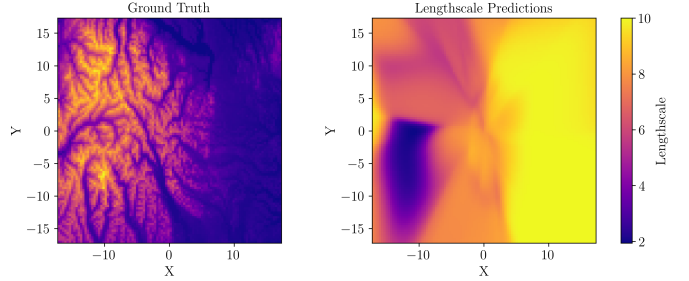


Fig. 4: Left: SRTM ground truth data from 47°N, 124°W. Right: Lengthscales from a non-stationary kernel.

VI. EXPERIMENTS

This section presents two sets of experiments. First, we benchmark the proposed methods on real-world data to evaluate performance and compare against a baseline approach with guaranteed estimation uncertainty. Second, we demonstrate real-world feasibility via field trials.

A. Benchmark Experiments

We benchmarked the proposed methods on the Shuttle Radar Topography Mission (SRTM) dataset [36], which provides high-resolution digital elevation data worldwide. We focused on the region near 47°N, 124°W, chosen for its complex, non-stationary spatial structure; results for three additional locations are reported in the Appendix. All benchmarks were run on a computer with an Intel i9-14900K CPU and 64 GB of RAM.

As a baseline, we used HEXCOVER [2], which produces informative path planning (IPP) solutions with guaranteed estimation uncertainty. We compared HEXCOVER against GREEDYCOVER (Section V-C) and GCBCOVER (Section V-D). GCBCOVER was evaluated both with and without an explicit distance budget. We used a non-stationary Attentive kernel [24], which models the field using a mixture of RBF kernels to capture spatially varying correlations. Since HEXCOVER is limited to a stationary RBF kernel, we set its lengthscale to the *smallest* lengthscale inferred by the trained Attentive kernel—a conservative choice that usually preserves the uncertainty guarantee.

We trained the Attentive kernel by fitting a Gaussian process (GP) [7] to data collected along an initial pilot path. The pilot path was generated by uniformly sampling locations in the domain \mathcal{X} , clustering these samples using k -means [37], and selecting the resulting cluster centroids as waypoints. We used 10 waypoints for the pilot path, then computed a route through them with a Traveling Salesperson Problem (TSP) solver [31]. We collected 350 measurements along this pilot path to initialize the GP. Figure 4 shows the SRTM ground truth for 47°N, 124°W, along with the spatially varying lengthscales learned by the Attentive kernel. The learned kernel function and likelihood noise variance were then provided to each planner to generate solution paths with guaranteed estimation uncertainty.

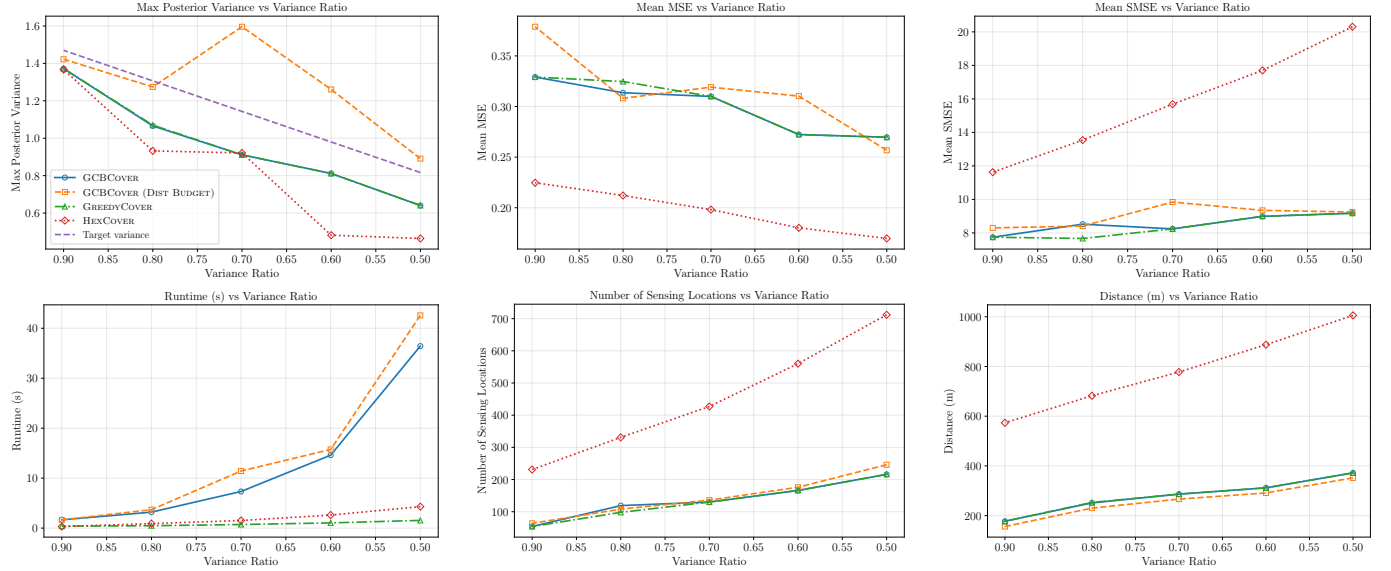


Fig. 5: Benchmark results on SRTM at 47°N, 124°W. Top row: resulting maximum posterior variance, MSE, and SMSE. Bottom row: runtime, number of selected sensing locations, and total path length. GREEDYCOVER and GCBCOVER achieve the target uncertainty with fewer waypoints and shorter paths than HEXCOVER, while distance-budgeted GCBCOVER trades variance reduction to satisfy the travel distance budget.

None of the planning methods explicitly account for measurements collected from the pilot path; during planning, they use only the learned kernel and noise variance. GREEDYCOVER and GCBCOVER can be warm-started by seeding the selected sensing locations with already visited points and then planning the remaining route, potentially reducing the number of additional waypoints (and thus total travel distance). However, HEXCOVER does not support such initialization. For a consistent comparison, we therefore incorporate the pilot measurements only during evaluation, not during planning.

For each dataset, we used the GP trained on the pilot data to compute the maximum posterior variance over a discrete evaluation grid covering the environment. We then set the target variance threshold as a fixed fraction of this maximum, sweeping the fraction from 0.9 down to 0.5. For GCBCOVER in the distance-budgeted setting, we set the budget to the length of GCBCOVER’s unconstrained solution minus 20 m. This ties the budget to the travel distance required to meet the uncertainty constraint while introducing a meaningful shortfall that stresses the budgeted planner.

To evaluate each method, we combined measurements from the pilot path with those collected at the solution waypoints and computed six metrics: (i) maximum posterior variance, (ii) mean squared error (MSE) [7], (iii) standardized mean squared error (SMSE) [7], (iv) algorithm runtime, (v) number of selected sensing locations (waypoints), and (vi) total solution path length. Figure 5 reports benchmark results for 47°N, 124°W. Additional results are provided in the Appendix along with representative solution paths.

Across the full range of threshold ratios, all methods satisfy the target variance requirement, except for distance-budgeted GCBCOVER, which trades variance reduction to ensure the

imposed travel distance limit. HEXCOVER achieves the lowest maximum posterior variance and shows a similar advantage in MSE. In contrast, the SMSE results suggest that GREEDYCOVER and GCBCOVER yield better calibrated, uncertainty-aware predictions.

Runtime also differs substantially across methods. GREEDYCOVER is consistently faster than HEXCOVER. For HEXCOVER, sensing-location selection takes less than a second in all evaluations; the TSP solver dominates the overall runtime. This is partly because HEXCOVER selects more sensing locations than GREEDYCOVER, increasing routing complexity. GCBCOVER is noticeably slower due to its tighter coupling between selection and routing. This additional computation enables GCBCOVER to enforce a strict distance constraint while retaining a near-optimal approximation guarantee for the joint sensing-location selection and routing problem.

From a deployment perspective, the most relevant metrics are the number of sensing locations and the resulting path length. GREEDYCOVER and GCBCOVER consistently require fewer waypoints and less travel to achieve the same target maximum variance. This improvement stems from two factors: the Attentive kernel captures non-stationarity in the underlying field, and the planners leverage the spatially varying correlations to prioritize the most informative sensing locations.

B. Autonomous Surface Vehicle Field Trial

We validated the proposed method in a real-world deployment using a custom-built autonomous surface vehicle (ASV) to map lake bathymetry. The monitoring region was restricted to a non-convex subset of the lake. The ASV platform (Figure 2) was equipped with GPS, a single-beam sonar, and a Raspberry Pi 5 for onboard computation.

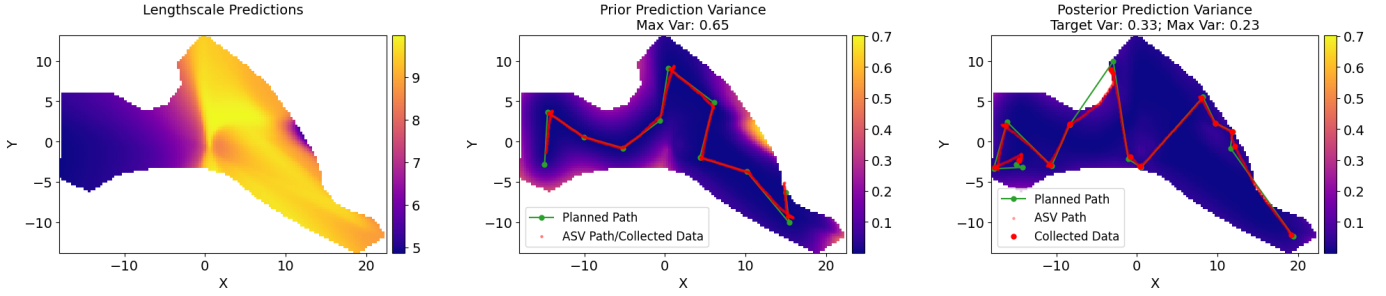


Fig. 6: Autonomous surface vehicle field-trial results using GREEDYCOVER. Left: lengthscales from the learned non-stationary kernel. Middle: GP prior predictive variance with the initial path data. Right: GP posterior predictive variance after conditioning on IPP solution data.

We conducted an IPP trial using GREEDYCOVER. We first generated a pilot path with ten waypoints via k -means and collected 544 depth measurements along this path. Using this data, we fit a GP with an Attentive kernel [24]. We set the target maximum posterior variance to (50%) of the maximum variance obtained after executing the pilot path, and then computed the IPP solution. To accelerate convergence and reduce path length, we warm-started GREEDYCOVER with the pilot data. Consequently, the planned IPP solution avoided revisiting locations near the pilot path and prioritized regions whose uncertainty remained above the target threshold. After executing the IPP solution, we updated the GP using measurements collected *only at the visited waypoints* and evaluated the resulting maximum posterior variance. Additional implementation details are provided in the code Appendix. The learned lengthscales, together with the planned and executed pilot and informative paths, are shown in Figure 6.

Despite deviations from the planned path, the method successfully reduced uncertainty such that the maximum-variance threshold was satisfied over the monitoring region. We also observed that the IPP sensing locations remained within the region boundary, and the low-level trajectory planner [38] adjusted the executed path to remain inside the non-convex domain, consistent with the non-convex domain constraints. Details of the ocean field trial with an Aqua2 autonomous underwater vehicle (AUV) [39] are provided in the Appendix.

VII. LIMITATIONS

A central limitation is the reliance on a well-specified GP kernel: if the kernel is misspecified, the bound on predictive variance may fail to be a strict lower bound on the true mean-squared prediction error. An important extension is *online* operation that adapts a non-stationary kernel from streaming data (e.g., POAM [25]) and provides guarantees that are robust to bounded hyperparameter or model uncertainty. Alternatively, correlations could be inferred from physics-based priors or historical data, reducing—or potentially eliminating—the need for pilot data collection and onboard kernel learning.

Second, our guarantees are enforced on a finite evaluation set \mathcal{V} and therefore may not hold uniformly over the continuous domain. Future work could exploit regularity of the GP variance (e.g., continuity or Lipschitz properties) to guide

grid-resolution selection and lift guarantees from \mathcal{V} to the continuous domain.

Finally, the field trials highlight execution uncertainty (e.g., localization error and imperfect tracking). Incorporating these effects via chance-constrained formulations would further improve real-world reliability.

VIII. CONCLUSION

We presented two planners for *informative path planning (IPP) with guaranteed estimation uncertainty* that compute near-shortest (or budget-feasible) sensing paths whose measurements ensure that the Gaussian process (GP) posterior variance at every evaluation point falls below a user-specified threshold. This provides coverage-style guarantees while leveraging correlation-aware sampling.

To make the problem tractable, we fit a GP to available prior information and construct *binary coverage maps* by thresholding kernel-induced covariance, reducing the global variance requirement to a discrete coverage problem over evaluation points. This reduction enables efficient planning with guarantees: GREEDYCOVER yields a near-optimal approximation for selecting sensing locations, while GCBCOVER balances marginal coverage gain against marginal path length to obtain near-optimal solutions under a strict distance budget. Unlike geometric sweep patterns, both methods adapt sampling to the learned correlation structure.

The approach supports *non-stationary* fields via non-stationary kernels, concentrating measurements in high-variation regions while avoiding redundant sampling in smooth, predictable areas, and it naturally extends to *non-convex* domains with obstacles. Experiments on SRTM topography show that GREEDYCOVER and GCBCOVER satisfy the maximum-variance constraint while reducing measurements and travel distance relative to a coverage-guaranteed baseline. We also demonstrated GREEDYCOVER in field trials with bathymetry-mapping autonomous surface and underwater vehicles, establishing real-world feasibility.

Future work includes IPP with guaranteed estimation uncertainty that accommodates vehicle dynamics, motion uncertainty, continuous sensing, and decentralized multi-robot deployments that scale to large environments under limited communication.

REFERENCES

- [1] Kalvik Jakkala and Srinivas Akella. **Fully differentiable sensor placement and informative path planning**. *The International Journal of Robotics Research*, 2025.
- [2] Shamak Dutta, Nils Wilde, Pratap Tokekar, and Stephen L. Smith. **Approximation Algorithms for Robot Tours in Random Fields with Guaranteed Estimation Accuracy**. In *2023 IEEE International Conference on Robotics and Automation (ICRA)*, pages 7830–7836, 2023.
- [3] Gary M. Lovett, Douglas A. Burns, Charles T. Driscoll, Jennifer C. Jenkins, Myron J. Mitchell, Lindsey Rustad, James B. Shanley, Gene E. Likens, and Richard Haeuber. **Who needs environmental monitoring?** *Frontiers in Ecology and the Environment*, 5(5):253–260, 2007.
- [4] Howie Choset and Philippe Pignon. **Coverage Path Planning: The Boustrophedon Cellular Decomposition**. In *Field and Service Robotics*, pages 203–209, London, 1998. Springer London.
- [5] Nare Karapetyan, Jason Moulton, Jeremy S. Lewis, Alberto Quattrini Li, Jason M. O’Kane, and Ioannis M. Rekleitis. **Multi-robot Dubins Coverage with Autonomous Surface Vehicles**. *2018 IEEE International Conference on Robotics and Automation (ICRA)*, pages 2373–2379, 2018.
- [6] Saurav Agarwal and Srinivas Akella. **Area Coverage With Multiple Capacity-Constrained Robots**. *IEEE Robotics and Automation Letters*, 7(2):3734–3741, 2022.
- [7] Carl Edward Rasmussen and Christopher K. I. Williams. *Gaussian Processes for Machine Learning*. MIT Press, Cambridge, USA, 2005.
- [8] Varun Suryan and Pratap Tokekar. **Learning a Spatial Field in Minimum Time With a Team of Robots**. *IEEE Transactions on Robotics*, 36(5):1562–1576, 2020.
- [9] H. González-Banos and Jean-Claude Latombe. **A Randomized Art-Gallery Algorithm for Sensor Placement**. In *Proceedings of the Seventeenth Annual Symposium on Computational Geometry*, page 232–240, New York, NY, USA, 2001.
- [10] Andreas Breitenmoser, Mac Schwager, Jean-Claude Metzger, Roland Siegwart, and Daniela Rus. **Voronoi coverage of non-convex environments with a group of networked robots**. In *2010 IEEE International Conference on Robotics and Automation*, pages 4982–4989, 2010.
- [11] Mac Schwager, Michael P. Vitus, Samantha Powers, Daniela Rus, and Claire J. Tomlin. **Robust Adaptive Coverage Control for Robotic Sensor Networks**. *IEEE Transactions on Control of Network Systems*, 4(3), 2017.
- [12] Amanda Bouman, Joshua Ott, Sung-Kyun Kim, Kenny Chen, Mykel J. Kochenderfer, Brett Lopez, Ali-akbar Agha-mohammadi, and Joel Burdick. **Adaptive Coverage Path Planning for Efficient Exploration of Unknown Environments**. In *2022 IEEE/RSJ International Conference on Intelligent Robots and Systems (IROS)*, pages 11916–11923, 2022.
- [13] Andreas Krause, Ajit Singh, and Carlos Guestrin. **Near-Optimal Sensor Placements in Gaussian Processes: Theory, Efficient Algorithms and Empirical Studies**. *Journal of Machine Learning Research*, 9(8):235–284, 2008.
- [14] Chandra Chekuri and M. Pal. **A recursive greedy algorithm for walks in directed graphs**. In *46th Annual IEEE Symposium on Foundations of Computer Science (FOCS’05)*, pages 245–253, 2005.
- [15] Lorenzo Bottarelli, Manuele Bicego, Jason Blum, and Alessandro Farinelli. **Orienteering-based informative path planning for environmental monitoring**. *Engineering Applications of Artificial Intelligence*, 77:46 – 58, 2019.
- [16] Jonathan Binney, Andreas Krause, and Gaurav S. Sukhatme. **Optimizing waypoints for monitoring spatiotemporal phenomena**. *The International Journal of Robotics Research*, 32(8):873–888, 2013.
- [17] Gregory Hitz, Enric Galceran, Marie-Eve Garneau, François Pomerleau, and Roland Siegwart. **Adaptive continuous-space informative path planning for online environmental monitoring**. *Journal of Field Robotics*, 34(8):1427–1449, 2017.
- [18] Gilad Francis, Lionel Ott, Roman Marchant, and Fabio Ramos. **Occupancy map building through Bayesian exploration**. *The International Journal of Robotics Research*, 38(7):769–792, 2019.
- [19] Joshua Ott, Mykel J. Kochenderfer, and Stephen Boyd. **Approximate sequential optimization for informative path planning**. *Robotics and Autonomous Systems*, 182: 104814, 2024.
- [20] Ananya Rao, Howie Choset, and David Wettergreen. **Wavelet-Based Distributed Coverage for Heterogeneous Agents**. In *2025 IEEE International Conference on Robotics and Automation (ICRA)*, pages 6630–6637, 2025.
- [21] Julius Rückin, Liren Jin, and Marija Popović. **Adaptive Informative Path Planning Using Deep Reinforcement Learning for UAV-based Active Sensing**. In *2022 International Conference on Robotics and Automation (ICRA)*, pages 4473–4479, 2022.
- [22] Jose Fuentes, Paulo Padrão, Abdullah Al Redwan Newaz, and Leonardo Bobadilla. **Learning-Based Adaptive Navigation for Scalar Field Mapping and Feature Tracking**. In *2025 IEEE International Conference on Robotics and Automation (ICRA)*, pages 1–7, 2025.
- [23] Sandeep Manjanna and Gregory Dudek. **Data-driven selective sampling for marine vehicles using multi-scale paths**. In *2017 IEEE/RSJ International Conference on Intelligent Robots and Systems (IROS)*, 2017.
- [24] Weizhe Chen, Roni Khordon, and Lantao Liu. **AK: Attentive Kernel for Information Gathering**. In *Proceedings of Robotics: Science and Systems*, New York City, NY, USA, June 2022.
- [25] Weizhe Chen, Lantao Liu, and Roni Khordon. **POAM: Probabilistic Online Attentive Mapping for Efficient Robotic Information Gathering**. In *Robotics: Science and Systems*, 2024.

[26] Kalvik Jakkala and Srinivas Akella. [Multi-Robot Informative Path Planning from Regression with Sparse Gaussian Processes](#). In *2024 IEEE International Conference on Robotics and Automation (ICRA)*, 2024.

[27] Kalvik Jakkala and Srinivas Akella. [Fully Differentiable Adaptive Informative Path Planning](#). In *2025 IEEE International Conference on Robotics and Automation*, pages 5431–5437, Atlanta, GA, May 2025.

[28] Kalvik Jakkala and Srinivas Akella. [Probabilistic Gas Leak Rate Estimation Using Submodular Function Maximization With Routing Constraints](#). *IEEE Robotics and Automation Letters*, 7(2):5230–5237, 2022.

[29] Johan Wagberg, Dave Zachariah, Thomas Schon, and Petre Stoica. [Prediction Performance After Learning in Gaussian Process Regression](#). In *Proceedings of the 20th International Conference on Artificial Intelligence and Statistics*, volume 54 of *Proceedings of Machine Learning Research*, pages 1264–1272. PMLR, 20–22 Apr 2017.

[30] Marc Häkkinen, Markus Lange-Hegermann, and Bogdan Raită. [Gaussian Process Priors for Systems of Linear Partial Differential Equations with Constant Coefficients](#). In *Proceedings of the 40th International Conference on Machine Learning*, ICML. JMLR, 2023.

[31] Nicos Christofides. [Worst-Case Analysis of a New Heuristic for the Travelling Salesman Problem](#). *Operations Research Forum*, 3(1):20, Mar 2022.

[32] G. L. Nemhauser, L. A. Wolsey, and M. L. Fisher. [An analysis of approximations for maximizing submodular set functions-I](#). *Mathematical Programming*, 14(1):265–294, Dec 1978.

[33] K.M. Lynch and F.C. Park. [Modern Robotics](#). Cambridge University Press, 2017.

[34] Haifeng Zhang and Yevgeniy Vorobeychik. [Submodular Optimization with Routing Constraints](#). In *Proceedings of the Thirtieth AAAI Conference on Artificial Intelligence*, page 819–825, 2016.

[35] Pao-Te Lin and Kuo-Shih Tseng. [Improvement of Submodular Maximization Problems With Routing Constraints via Submodularity and Fourier Sparsity](#). *IEEE Robotics and Automation Letters*, 8(4):1927–1934, 2023.

[36] Tom G Farr, Paul A Rosen, Edward Caro, Robert Crippen, Riley Duren, Scott Hensley, Michael Kobrick, Mimi Paller, Ernesto Rodriguez, Ladislav Roth, et al. [The Shuttle Radar Topography Mission](#). *Reviews of geophysics*, 45(2), 2007.

[37] C.M. Bishop. [Pattern Recognition and Machine Learning](#). Information Science and Statistics. Springer New York, 2006.

[38] Anders Strand-Holm Vinther and Anders Strand-Holm Magnus. [Pathfinding in Two-dimensional Worlds](#). Master’s thesis, Aarhus University, 2015.

[39] Gregory Dudek, Philippe Giguere, Chris Prahalas, Shane Saunderson, Junaed Sattar, Luz-abril Torres-Mendez, Michael Jenkin, Andrew German, Andrew Hogue, Arlene Ripsman, Jim Zacher, Evangelos Miliros, Hui Liu, Pifu Zhang, Marti Buehler, and Christina Georgiades. [AQUA: An Amphibious Autonomous Robot](#). *Computer*, 40(1):46–53, 2007.

[40] T.M. Cover and J.A. Thomas. [Elements of Information Theory](#). Wiley Series in Telecommunications and Signal Processing. Wiley, 1991.

APPENDIX

A. Theorems and Proofs

This appendix collects theoretical details that support our approaches.

a) Coverage-map construction: The binary coverage maps used by GREEDYCOVER and GCBCOVER are constructed by evaluating whether a *single* candidate sensing location c can reduce the posterior variance at an evaluation point v below the target threshold σ_{tar}^2 . Theorem 1 gives an explicit covariance threshold for this single-location condition. Theorem 2 shows that this condition is *conservative but safe*: conditioning on additional sensing locations cannot increase posterior variance, so any point covered under the single-location test remains covered under multi-location conditioning.

Theorem 1 (Minimum Required Prior Covariance).

Let $f \sim \mathcal{GP}(0, k)$ with independent Gaussian observation noise variance σ_n^2 , and consider a single noisy observation at candidate location $c \in \mathcal{C}$. Fix an evaluation location $v \in \mathcal{V}$. For any target posterior variance $\sigma_{\text{tar}}^2 \in (0, k(v, v))$, the condition

$$\sigma_{\text{post}}^2(v | c) \leq \sigma_{\text{tar}}^2$$

holds if and only if

$$|k(c, v)| \geq \sqrt{(k(v, v) - \sigma_{\text{tar}}^2)(k(c, c) + \sigma_n^2)}. \quad (10)$$

Thus, achieving a posterior variance of at most σ_{tar}^2 at v requires that the prior covariance between c and v exceed the threshold in Equation 8.

Proof: Define $k_{cc} = k(c, c)$, $k_{cv} = k(c, v)$, and $k_{vv} = k(v, v)$. The pair $(f(c), f(v))$ is jointly Gaussian with covariance

$$\Sigma = \begin{bmatrix} k_{cc} & k_{cv} \\ k_{cv} & k_{vv} \end{bmatrix}.$$

With observation noise variance σ_n^2 , the Gaussian conditioning identity gives

$$\sigma_{\text{post}}^2(v | c) = k_{vv} - \frac{k_{cv}^2}{k_{cc} + \sigma_n^2}. \quad (11)$$

Requiring $\sigma_{\text{post}}^2(v | c) \leq \sigma_{\text{tar}}^2$ is equivalent to

$$k_{cv}^2 \geq (k_{vv} - \sigma_{\text{tar}}^2)(k_{cc} + \sigma_n^2).$$

Taking square roots yields Equation 8. \blacksquare

Theorem 2 (Variance Reduction with Multiple Locations).

Under the setup of Theorem 1, consider n sensing locations $c_1, \dots, c_n \in \mathcal{C}$. Fix an evaluation location $v \in \mathcal{V}$ and a target variance $\sigma_{\text{tar}}^2 \in (0, k(v, v))$. Suppose there exists $j \in \{1, \dots, n\}$ such that

$$|k(c_j, v)| \geq \sqrt{(k(v, v) - \sigma_{\text{tar}}^2)(k(c_j, c_j) + \sigma_n^2)}.$$

Then the posterior variance at v conditioned on all observations satisfies

$$\sigma_{\text{post}}^2(v | c_{1:n}) \leq \sigma_{\text{tar}}^2.$$

Proof: By assumption, there exists c_j such that $\sigma_{\text{post}}^2(v | c_j) \leq \sigma_{\text{tar}}^2$. For jointly Gaussian variables, conditional variance is monotone non-increasing under additional conditioning: if (U, V, W) are jointly Gaussian, then

$$\sigma_{\text{post}}^2(U | V, W) \leq \sigma_{\text{post}}^2(U | V),$$

which follows from the fact that conditioning reduces entropy [40, Theorem 2.6.5]. Applying this property yields

$$\sigma_{\text{post}}^2(v | c_{1:n}) \leq \sigma_{\text{post}}^2(v | c_j) \leq \sigma_{\text{tar}}^2. \quad \blacksquare$$

b) Coverage objective vs. joint posterior uncertainty:

It is important to distinguish the *coverage objective* F from the underlying uncertainty-reduction mechanism used to construct the coverage sets. In our coverage-map construction (Section V-B), each candidate j is associated with a fixed set of covered points computed in isolation (i.e., by conditioning on a single candidate at a time). This induces the union-of-sets objective in Equation 9, which is monotone submodular and therefore admits the $(1 - 1/e)$ approximation guarantee described below.

When multiple sensing locations are chosen together, their joint impact on posterior uncertainty can be *super-additive*: some evaluation points fall below the uncertainty threshold only after conditioning on several locations at once. Because these interaction effects are not captured by per-candidate coverage sets, the resulting estimate $F(S)$ is conservative. This conservatism works in our favor: if the algorithm reports that a set S meets a target coverage level under the isolated-candidate model, then the *true* maximum posterior variance after executing S is typically no greater—and often strictly lower—than the target threshold.

A tighter (but more expensive) alternative is to recompute the true achieved coverage at each iteration by evaluating the GP posterior variance over the evaluation set under the current selection S_t , and then updating coverage accordingly (Algorithm 1, line 13). This explicitly captures joint (multi-location) effects rather than relying on per-candidate coverage.

c) Background approximation results (Theorems 3–4):

The next two theorems are foundational results used to justify the approximation guarantees of the greedy coverage maximization and the generalized cost–benefit (GCB) selection approach. We restate them for completeness; their proofs are available in the cited references.

Theorem 3 (Nemhauser et al., 1978 [32]).

Let F be a monotone submodular set function over a finite ground set \mathcal{V} with $F(\emptyset) = 0$. Let \mathcal{A}_G be the set of the first k elements chosen by the greedy algorithm, and let $\text{OPT} = \max_{\mathcal{A} \subset \mathcal{V}, |\mathcal{A}|=k} F(\mathcal{A})$. Then

$$F(\mathcal{A}_G) \geq \left(1 - \left(\frac{k-1}{k}\right)^k\right) \text{OPT} \geq (1 - 1/e) \text{OPT}.$$

Theorem 4 (Zhang and Vorobeychik, 2016 [34]).
The GCB algorithm obtains a set X such that

$$f(X) \geq \frac{1}{2}(1 - 1/e)f(\tilde{X}),$$

where \tilde{X} is the optimal solution of

$$\max \left\{ f(X) \mid c(X) \leq \frac{\alpha B(1 + \alpha(K_c - 1)(1 - k_c))}{\psi(n) K_c} \right\},$$

and \hat{c} is an α -submodular $\psi(n)$ -approximation of an α -submodular function c .

B. Algorithms: Coverage-Based Selection and Path Planning

This subsection provides pseudocode for the two planners presented in the paper. Both algorithms operate on a binary coverage matrix $B \in \{0, 1\}^{M \times N}$ constructed from the learned GP kernel via the covariance threshold in Theorem 1. The matrix entry $B_{ji} = 1$ indicates that sensing at candidate location c_j is sufficient (under the single-location test) to reduce posterior variance at evaluation point v_i below σ_{tar}^2 .

We use both index-set and location-set notation interchangeably. For example, a sensing set may be written as an index set $S \subseteq \{1, \dots, M\}$ or as the corresponding location set $\{c_j : j \in S\} \subseteq \mathcal{C}$. The intended meaning is clear from context.

a) **GREEDYCOVER**: Algorithm 1 greedily selects sensing locations to maximize the monotone submodular coverage objective $F(S)$ (Equation 9) by repeatedly choosing the candidate that covers the largest number of currently uncovered evaluation points.

Algorithm 1 GREEDYCOVER: Estimation Uncertainty Guaranteed Sensor Placement

Require: Coverage matrix $B \in \{0, 1\}^{M \times N}$; evaluation set $\mathcal{V} = \{v_1, \dots, v_N\}$.
Ensure: Selected index set $S \subseteq \{1, \dots, M\}$.
1: $S \leftarrow \emptyset$ ▷ selected sensing-location indices
2: $U \leftarrow \emptyset$ ▷ covered evaluation points
3: **while** $|U| < N$ **do**
4: **for** each candidate $j \in \{1, \dots, M\} \setminus S$ **do**
5: $g(j) \leftarrow |\{v_i \in \mathcal{V} : B_{ji} = 1, v_i \notin U\}|$
6: ▷ marginal gain
7: **end for**
8: $j^* \leftarrow \arg \max_j g(j)$
9: **if** $g(j^*) = 0$ **then**
10: **break** ▷ no further improvement possible
11: **end if**
12: $S \leftarrow S \cup \{j^*\}$
13: $U \leftarrow U \cup \{v_i \in \mathcal{V} : B_{j^*i} = 1\}$
14: **end while**
15: **return** S

b) **GCBCOVER**: Algorithm 2 extends GREEDYCOVER to the routing-constrained setting by selecting candidates based on a coverage-per-distance ratio. It also computes a (truncated) greedy-coverage baseline and returns the better of the two, consistent with the GCB algorithm.

Algorithm 2 GCBCOVER: Estimation Uncertainty Guaranteed Informative Path Planning

Require: Coverage matrix $B \in \{0, 1\}^{M \times N}$, distance budget D .
Ensure: Selected ordered index set $S \subseteq \{1, \dots, M\}$.
1: $S_{\text{Greedy}} \leftarrow \text{GREEDYCOVER}(B)$ ▷ Algorithm 1
2: Compute a route $\mathcal{P}_{\text{Greedy}}$ through $\{c_j : j \in S_{\text{Greedy}}\}$ and truncate it to length $\leq D$
3: Let S_{Greedy} be the indices visited by the truncated route
4: $S \leftarrow \emptyset; U \leftarrow \emptyset$ ▷ current selection and covered set
5: **while** $\text{length}(S) \leq D$ **and** $|U| < N$ **do**
6: **for all** $j \in \{1, \dots, M\} \setminus S$ **do**
7: $\Delta F_j \leftarrow F(S \cup \{j\}) - F(S)$
8: $\Delta \text{length}_j \leftarrow \text{length}(S \cup \{j\}) - \text{length}(S)$
9: $r(j) \leftarrow \Delta F_j / \Delta \text{length}_j$
10: **end for**
11: $j^* \leftarrow \arg \max_j r(j)$
12: **if** $\text{length}(S \cup \{j^*\}) \leq D$ **then**
13: $S \leftarrow S \cup \{j^*\}; U \leftarrow U \cup \{v_i : B_{j^*i} = 1\}$
14: **end if**
15: Remove j^* from future consideration
16: **end while**
17: **return** $\arg \max_{A \in \{S_{\text{Greedy}}, S\}} F(A)$

C. Routing-Cost Heuristic and Computational Efficiency

The GCB selection rule requires evaluating the marginal routing-cost increment $\Delta \text{length}(j \mid S)$ for many candidate additions. A naive implementation would repeatedly solve a routing problem (e.g., a TSP) for each candidate at each iteration, which is computationally expensive.

To reduce the number of full routing solves, we estimate $\Delta \text{length}(j \mid S)$ using a fast nearest-insertion heuristic: we consider inserting the new location c_j along each edge of the current route and take the best (smallest) increase in route length. This yields an efficient approximation $\Delta \text{length}(j \mid S)$ that can be computed quickly for all candidates.

Algorithm 3 Approximate route increment (nearest-insertion heuristic)

1: **function** APPROXROUTEINCREMENT(j, S, \mathcal{P}_S)
2: Let \mathcal{P}_S be the current route visiting $\{c_k : k \in S\}$.
3: Initialize $\hat{c} \leftarrow \infty$.
4: **for** each edge (c_a, c_b) along \mathcal{P}_S **do**
5: Consider inserting c_j between c_a and c_b .
6: $\hat{c}_{ab} \leftarrow \text{length}(\mathcal{P}_S) + \|c_a - c_j\|$
7: $+ \|c_j - c_b\| - \|c_a - c_b\|$.
8: $\hat{c} \leftarrow \min(\hat{c}, \hat{c}_{ab})$.
9: **end for**
10: **return** $\hat{c} - \text{length}(\mathcal{P}_S)$.
11: **end function**

In the full GCBCOVER procedure, we therefore: (i) compute approximate increments for all candidates to rank them by the coverage-per-distance ratio, and (ii) invoke the exact

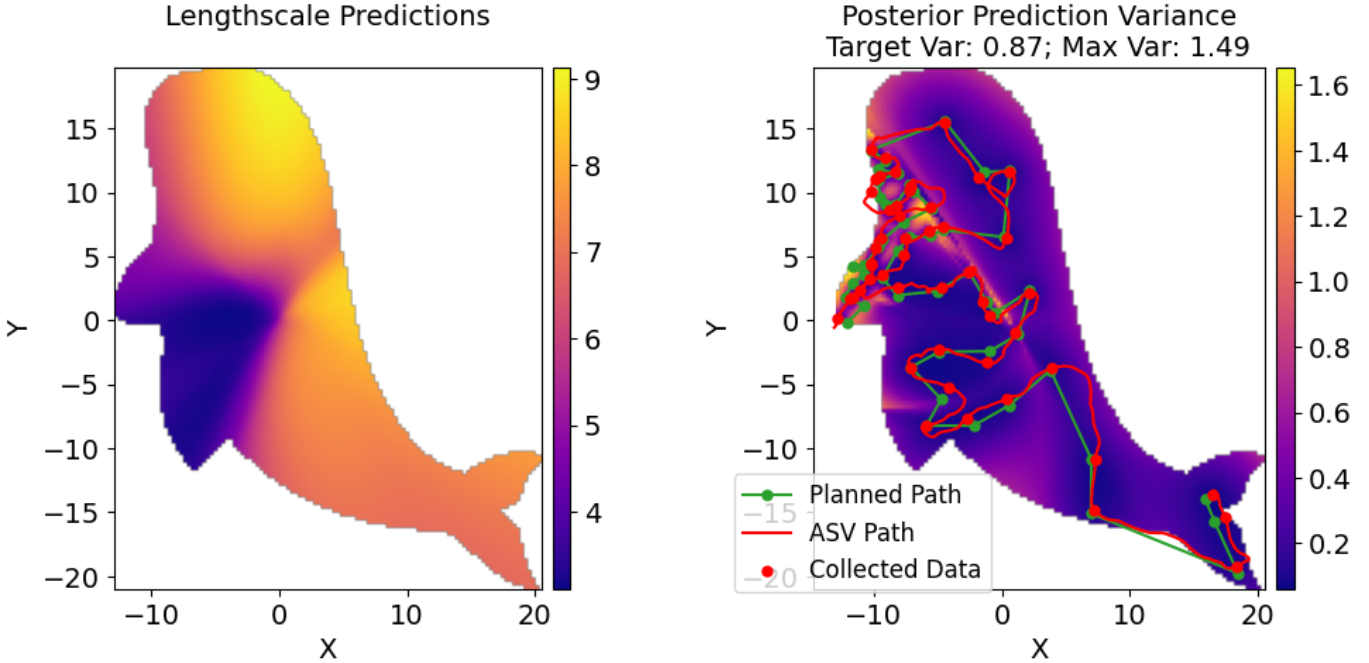


Fig. 7: Autonomous underwater vehicle field-trial results using GREEDYCOVER. Left: lengthscales from the learned non-stationary kernel. Right: GP posterior predictive variance after conditioning on IPP solution data.

routing solver only for the single top-ranked candidate to update the route and verify feasibility. This substantially reduces runtime while preserving the intended selection behavior (prioritizing high marginal coverage per unit travel).

D. Autonomous Underwater Vehicle Field Trial

We validated the proposed method in a real-world deployment using an Aqua2 autonomous underwater vehicle (AUV) [39] (Figure 2) to map ocean bathymetry in the Folkestone Marine Reserve, Barbados. Aqua2 is a non-holonomic robot that uses proportional-derivative (PD) controllers to actuate its six flippers for navigation. The monitoring region was restricted to a non-convex subset of the survey area. The vehicle was equipped with a Doppler velocity logger (DVL) to support navigation relative to the start location and to provide distance-to-ground measurements. During the trial, the vehicle was commanded to maintain a constant depth of 0.5 m below the surface.

We conducted an IPP trial using GREEDYCOVER. A GP with an Attentive kernel [24] was fit using preexisting data comprising 490 samples from the region. We set the target maximum posterior variance to 0.87 and computed the IPP solution. The solution was generated without warm starting; this choice produced a longer path, enabling us to better assess the impact of navigation uncertainty. Planning was performed offboard on a surface laptop. After executing the planned path, we updated the GP using measurements collected *only at the visited waypoints* and evaluated the resulting maximum posterior variance. The learned lengthscales, together with the planned and executed informative paths, are shown in Figure 7.

The vehicle remained close to the monitoring-region boundary, but we observed notable deviations from the planned path. We attribute these deviations to strong ocean currents and to the fact that the TSP solver did not account for vehicle motion constraints. Consequently, the execution did not achieve the target variance at every evaluation location within the region. Nonetheless, the collected data substantially reduced uncertainty in high-variance areas while minimizing travel distance by prioritizing locations with short lengthscales and high uncertainty.

E. Additional Benchmark Results

This section provides supplementary visualizations and results from the benchmarks.

Figure 8 shows representative solutions from each planner, illustrating the selected sensing locations, the resulting route, and the sensor field-of-view footprints. Figures 9–11 report additional benchmark results from different locations in the SRTM dataset.

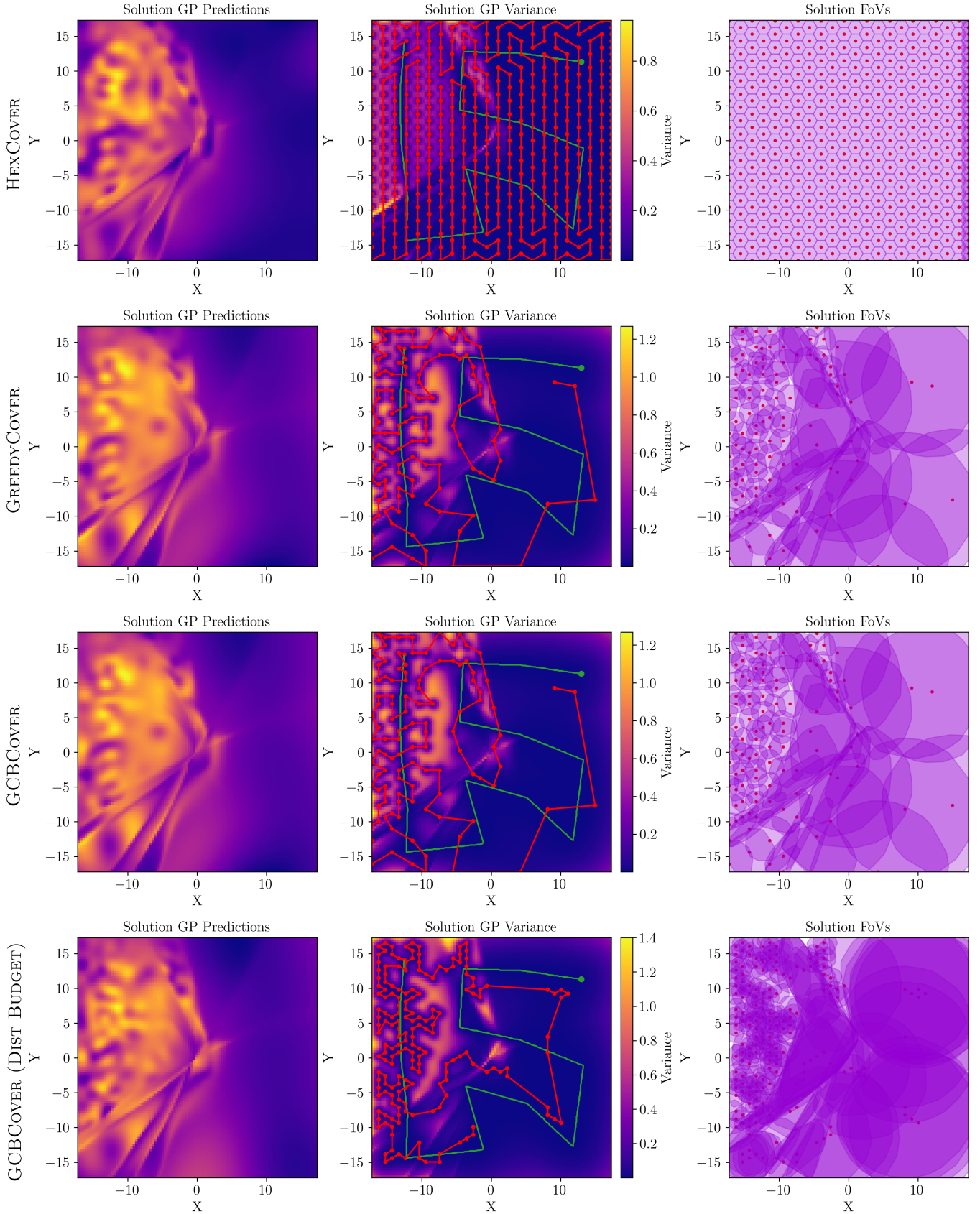


Fig. 8: Solutions from each approach with 0.7 variance ratio on SRTM dataset at 47°N , 124°W . Red points denote selected sensing locations. Red lines denote the planned informative path. The green line indicates the initial (pilot) data-collection path. Violet polygons depict the approximate sensor FoV footprint along the route.

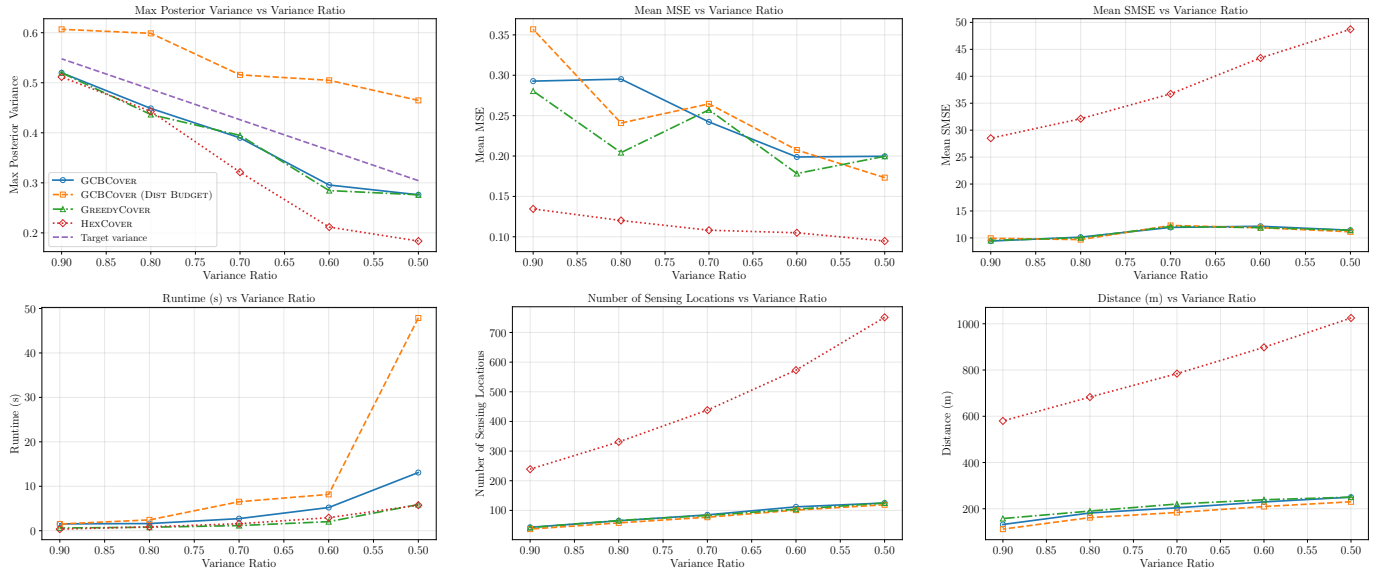


Fig. 9: Benchmark results on SRTM at 45°N, 123°W. We vary the target uncertainty threshold as a fraction of the maximum posterior variance after training on the pilot path (lower ratios correspond to stricter uncertainty requirements). Top row: resulting maximum posterior variance, MSE, and SMSE. Bottom row: runtime, number of selected sensing locations, and total path length

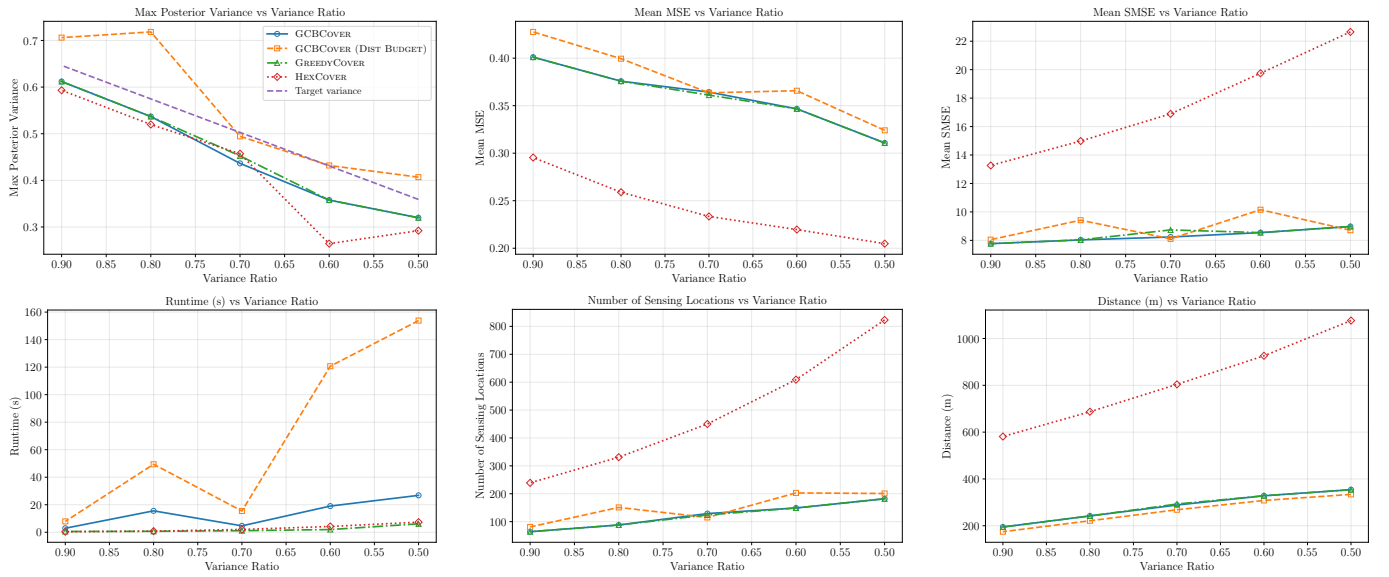


Fig. 10: Benchmark results on SRTM at 02°N, 021°W. We vary the target uncertainty threshold as a fraction of the maximum posterior variance after training on the pilot path (lower ratios correspond to stricter uncertainty requirements). Top row: resulting maximum posterior variance, MSE, and SMSE. Bottom row: runtime, number of selected sensing locations, and total path length

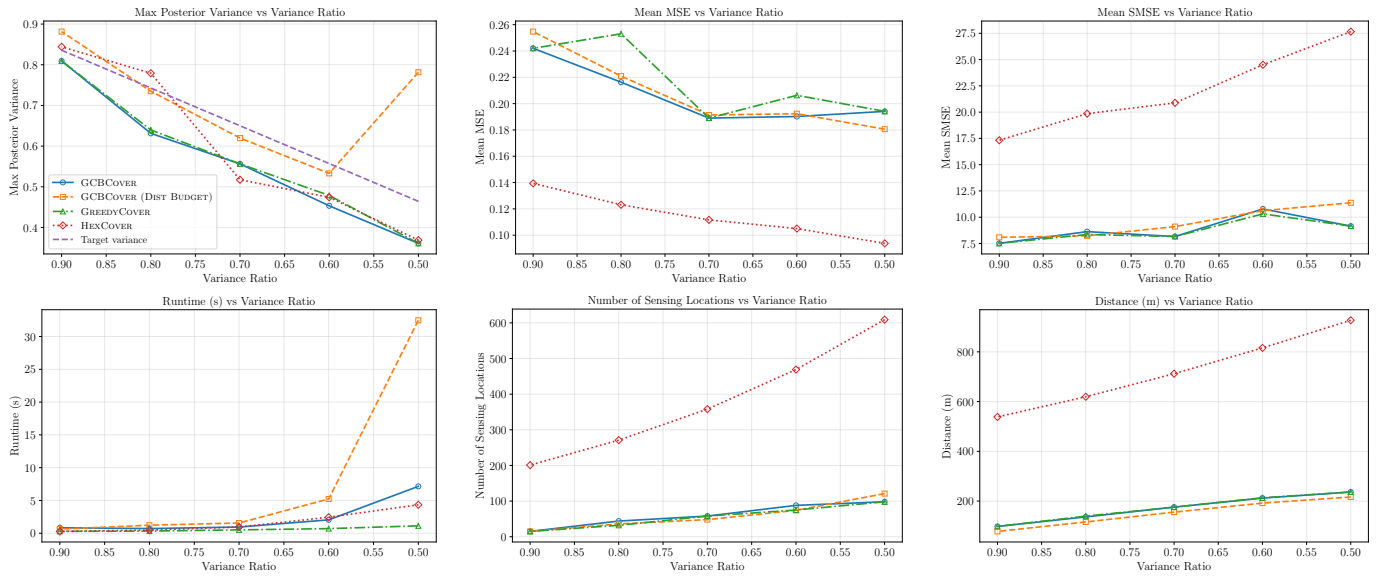


Fig. 11: Benchmark results on SRTM at 17°N, 073°W. We vary the target uncertainty threshold as a fraction of the maximum posterior variance after training on the pilot path (lower ratios correspond to stricter uncertainty requirements). Top row: resulting maximum posterior variance, MSE, and SMSE. Bottom row: runtime, number of selected sensing locations, and total path length